DOI: 10.61782/fa.2025.0275

FORUM ACUSTICUM EURONOISE 2025

DESIGN OF A METAMATERIAL PLATE WITH ACOUSTIC BLACK HOLE ABSORBERS AND ITS APPLICATION TO FLOATING RAFT SYSTEM

Siting Hao[1] **Haiqin Li**[1*] **Qian Ding**[1]
[1] Tianjin Key Laboratory of Nonlinear Dynamics and Control, Department of Mechanics, Tianjin University, China

ABSTRACT

Acoustic metamaterials have demonstrated great application potential in the fields of vibration and noise control. To suppress the broadband and low-frequency vibration in practical engineering, a novel design of the microunit is proposed, which uses a beam-type acoustic black hole (ABH) absorber as the resonator. By the coupling effects of ABH and the local resonance mechanism, a vibration attenuation band with relative bandwidth up to 0.93 can be generated. Furthermore, the microunit is used as the core layer embedded into a honeycomb raft plate, which is applied to the floating raft system. Due to the sandwich design, the stiffness of the novel metamaterial raft is improved. By analyzing the output vibration response of the foundation and the vibration level difference of the whole system, it shows a broadband and better vibration isolation performance, compared with the normal raft. In all, this study may provide a new idea for the design and application of vibration isolation meta-devices.

Keywords: acoustic metamaterial, acoustic black hole, floating raft system, vibration isolation.

1. INTRODUCTION

After the concept of acoustic black hole (ABH) was proposed by Mironov [1], the ABH-based structure has been studied extensively as a passive vibration control method [2]. Recent years, the idea of employing ABH-type structures as dynamic vibration absorbers (DVAs) has been emerged, proposed by Zhou and Cheng [3] first in the form of a unilateral ABH-DVA. Subsequently, various designs such as tree-shaped ABH-DVA [4] and two-dimensional circular ABH-DVA [5] are presented. Utilizing dynamic interaction with the host structure and damping enhancement as a result of ABH-specific energy trapping, resonant peaks can be reduced systematically over a broad frequency range, while the stiffness and strength of the host structure retain intact. Moreover, researchers introduce ABH-DVA into the concept of acoustic metamaterials, and demonstrate burgeoning potential in engineering vibration and noise reduction [6, 7]. For instance, the model and the corresponding calculation method of a host beam with distributed ABH-DVAs are proposed, achieving significant evanescent waves in a very broad frequency range [8, 9]. In research [10], discontinuous broadband vibration attenuation on a meta-beam is realized by using mistuning ABH-DVAs. However, studies for two-dimensional acoustic metamaterials with ABH-DVAs are not enough, and there is also a need for low-frequency vibration suppression.

Floating raft system is a typical vibration isolation technology used in ships and submarines, owing to its ability to inhibit the transmission of vibration generated by multiple equipment to the hull [11]. To further improve the vibration isolation performance of the system, various configurations have been added such as passive or active DVAs [12, 13], quasi-zero-stiffness (QZS) devices [14] and nonlinear energy sink (NES) cells [15]. However, the above studies either need complex structures or neglect the elastic deformation of the raft and foundation in modelling. Thus, some designs based on acoustic metamaterials have been proposed and focus on the substructures themselves in this coupled system. For example, a periodic structure is used to replace the isolators to suppress the disadvantageous effects

[*] ***Corresponding author***: lihaiqin1992@tju.edu.cn

of substructure resonances on vibration and noise radiation [16], while this may result in reduced stiffness which affects the practicability. Recent research designs a sandwich-plate-type raft with graded resonators, taking the advantage of light weight, high bending strength and high stiffness of sandwich structures [17]. Nevertheless, too much resonators may also add unnecessary load. Motivated by these studies, this paper aims to propose a light-weight sandwich raft plate to achieve low-frequency and broadband vibration isolation.

The rest of the paper is organized as follows. Section 2 presents the model of the metamaterial design based on ABH-DVA. Section 3 introduces both the numerical and experimental results of the vibration band gap, and the effect of ABH is analyzed. Section 4 illustrates the application of the proposed structure to the design of a sandwich raft, the static stiffness of which and the vibration isolation performance of the entire floating raft system are investigated. Finally, conclusions are drawn in Section 5.

2. MODELLING AND DESIGN

As depicted in Fig. 1, the proposed microunit is comprised of three parts: the inner ABH beam (the side view is shown in Fig. 1(c)), the outer frame, and the connectors in-between them. The whole structure is named as FC-ABH in the followings. The ABH beam is made of TPU (Thermoplastic Polyurethane), with width b (in the x direction) and assumed to undergo bending vibration in the z direction. Its layout in the y-z plane, see in Fig. 1(c), is symmetric about the horizontal line $y = 0$, as well as the mid-surface $z = 0$. As such, the ABH beam contains a plateau region of length $2l_0$ with uniform thickness and two thickness decreasing regions of length l_{ABH}, such that the overall thickness profile $h(y)$, as noted in Fig. 1(c), satisfying Eq. (1), where h_{min} and h_{uni} are respectively half of the thickness of the uniform region and the ABH terminal, and ε is the smooth parameter, defined by Eqn. (2).

$$h(y)=\begin{cases} 2h_{uni} & 0\le|y|\le l_0 \\ 2\left[h_{min}+\varepsilon\left(l_{ABH}+l_0-|y|^2\right)\right] & l_0\le|y|\le l_{ABH}+l_0 \end{cases} \quad (1)$$

$$\varepsilon=\frac{h_{uni}-h_{min}}{l_{ABH}^2} \quad (2)$$

Such an ABH beam is then embedded into a square frame through four identical connectors, each of whom is with thickness δ and with segment lengths l_1 (for segment ①), l_2 (for segment ②), and $(a\text{-}2\Delta a\text{-}b\text{-}2l_1\text{-}2\delta)/2$ (for segment ③). Both the frame and connectors are made of epoxy. All the geometric and material parameters are list in Tab. 1.

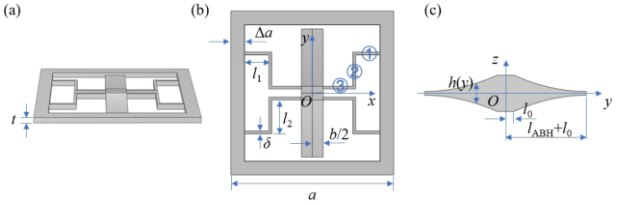

Figure 1. Schematic diagram of FC-ABH. (a) Stereogram of the microunit. (b) Top view. (c) Cross-section of the ABH portion.

Table 1. Structural parameters of FC-ABH. E_1, ρ_1, ν_1, E_2, ρ_2, ν_2 are elastic modulus, density and Poisson's ratio of epoxy and TPU respectively.

Parameters	Value[unit]	Parameters	Value[unit]
a	0.12[m]	h_{min}	0.5[mm]
Δa	0.01[m]	h_{uni}	0.002[m]
l_1	0.018[m]	l_{ABH}	0.042[m]
l_2	0.025[m]	l_0	0.005[m]
δ	0.002[m]	ε	0.85[m^{-1}]
t	0.003[m]	b	0.016[m]
E_1	2.6[GPa]	E_2	61[MPa]
ρ_1	1120[kg/m^3]	ρ_2	1100[kg/m^3]
ν_1	0.41	ν_2	0.47

3. VIBRATION ABSORPTION OF FC-ABH

3.1 Numerical simulation of bandgap

The Floquet-Bloch periodic boundary conditions are applied on the edges of the FC-ABH microunit as in Figs. (3) and (4), where $\boldsymbol{w}$ denotes the out-of-plane displacement vector, $\boldsymbol{k} = (k_x, k_y)$ is the wave vector and $i^2 = -1$[18].

$$\boldsymbol{w}\left(-\frac{a}{2},y\right)=\boldsymbol{w}\left(\frac{a}{2},y\right)e^{ik_x a} \quad (3)$$

$$\boldsymbol{w}\left(x,-\frac{a}{2}\right)=\boldsymbol{w}\left(x,\frac{a}{2}\right)e^{ik_y a} \quad (4)$$

The dispersion curve can be obtained by sweeping $\boldsymbol{k}$ along the boundaries of the irreducible Brillouin zone as shown in Fig. 2(a). The calculation process is carried out using the finite element method (FEM) via COMSOL, and the results are displayed by scatter points in Fig. 2(a). To manifest the dominant of flexural waves in vibration modes, the colors of these points are determined by Eqn. 5, where u and v are in-plane displacements along the x and y axes, and $\iiint$.dV

means that the integration is taken throughout the entire volume of the FC-ABH unit.

$$p = \frac{\iiint w^2 dV}{\iiint \left(u^2 + v^2 + w^2\right) dV} \tag{5}$$

It can be found that there is an omnidirectional bandgap within 61.29-68.78 Hz and several directional bandgaps within 68.78-90.82 Hz, 90.82-104.64 Hz and 119.3-167.12 Hz respectively.

To verify the predicted bandgaps by the dispersion curves, the vibration transmittance of a finite periodic plate consisting of 4 microunits is calculated. The model of the plate is shown in Fig. 2(b), with continuous periodicity boundary conditions applying in the y direction. Two specific points are noted: the bottom point EP denotes an excitation point where a unit harmonic force in the z direction is introduced into, while the top right point RP is the response point. By measuring the dynamic response of the two points, the transmittance is obtained as in Eqn. 6, where A_{out} and A_{in} are the acceleration amplitudes at RP and EP.

$$\text{Transmission} = 20\lg\frac{A_{out}}{A_{in}} \tag{6}$$

As presented in Fig. 2(b), there are three obvious vibration attenuation bands (named as VAB in the followings to distinguish from the bandgap), the frequency ranges of which are in good agreement with those of bandgaps in the dispersion curves. The relative bandwidth Ω of one VAB is defined as in Eqn. 7, where f_{upper} and f_{lower} represent the upper and lower boundary frequencies.

$$\Omega = \frac{2\left(f_{upper} - f_{lower}\right)}{f_{upper} + f_{lower}} \tag{7}$$

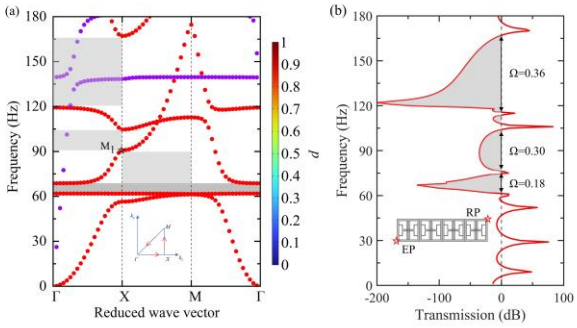

Figure 2. (a) Dispersion curves of the infinite periodic FC-ABH structure. (b) Transmittance of the finite periodic FC-ABH plate. The shaded areas indicate bandgaps or vibration attenuation bands (VABs).

3.2 Experimental validation

A vibration test is conducted to verify the transmittance results of numerical simulation. The 4×1 FC-ABH plate is manufactured by 3D printing, with the ABH portions printed using TPU while the others printed using polylactic acid (PLA). The experiment is carried out at room temperature, and it is noteworthy that the damping characteristics of the two materials are considered here. The material properties of PLA are E_3 = 1.98 GPa, ρ_3 = 1220 kg/m^3 and v_3 = 0.37, and the damping coefficients η of PLA and TPU are set as 0.1 and 0.15 respectively. Boundary conditions and the way of applying excitation are consistent with those set in the numerical simulation mentioned in subsection 3.1. Vibration signals are measured by the laser vibrometer (Ploytec PSV-500-3D).

Fig. 3 shows the experimental results, and the data is filtered using the moving average filter in MATLAB. It can be seen that there is a good agreement compared with the numerical results, especially for the frequency range of the VAB. Within the range of 0-150 Hz, a continuous VAB is generated beyond the third resonant frequency with Ω = 0.93, verifying the effective vibration suppression performance of the finite FC-ABH plate.

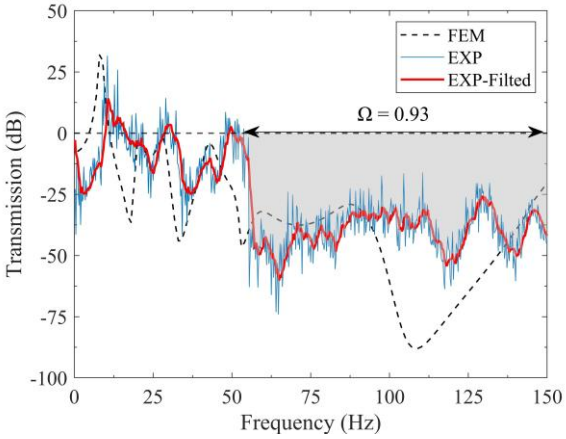

Figure 3. The experimental and simulation results of the transmittance of the finite periodic FC-ABH plate. The shaded area indicates the vibration attenuation band.

3.3 Effects of ABH

Since the bandgaps generated by FC-ABH are beyond the scope of conventional locally resonant bandgaps, one can deduce that the ABH beam acts a special role in the structure. In the view point of vibration absorption, ABH is generally proved to be effective beyond a certain cut-on frequency, which guarantees the tip to reduce the wave speed as well as the reflected energy. To make ABH perform sufficiently, the cut-on frequency is defined as in Eqn. (8) [19].

$$f_\varepsilon = \frac{\varepsilon}{\pi}\sqrt{\frac{3E_2}{4\rho_2}} = 55.17\text{Hz} \tag{8}$$

Therefore, for FC-ABH, ABH keeps absorbing vibration from the beginning of the first omnidirectional bandgap. This explains why the vibration can also be well attenuated at the frequency corresponding to M_1 marked in Fig. 2(a), although it is not within the bandgaps.

To illustrate this advantage more clearly, three frequency points are selected in the three VABs respectively, which are 65 Hz, 90 Hz and 130 Hz, and the displacement fields of the finite periodic plate at these frequencies are shown in Fig. 4. It can be observed that no matter inside or outside bandgaps, the displacement of the ABH portion is prominent, especially concentrated on the microunits near EP, thus reducing vibration at RP.

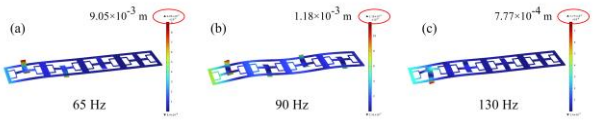

Figure 4. Displacement fields of the finite periodic FC-ABH plate at (a) 65 Hz, (b) 90 Hz and (c) 130 Hz.

4. APPLICATION TO FLOATING RAFT SYSTEM

Since the proposed FC-ABH can achieve broadband vibration suppression, in this section, it is used as the core layer embedded into a honeycomb plate. The periodic sandwich structure is then applied to the floating raft system, which can isolate the vibration transmitted by the machines to the hull effectively, under the premise of ensuring the load-bearing capacity.

4.1 Floating raft system based on FC-ABH

A typical model of the floating raft system is shown in Fig. 5(a), where the proposed FC-ABH is embedded into a conventional honeycomb plate-type raft periodically, forming a novel sandwich raft. The side length of the honeycomb microunit is equal to the lattice constant of the FC-ABH. Considering the practical application of this system, all parts of the raft and the foundation are made of structural steel. Parameters used in the calculation are depicted in Tab. 2.

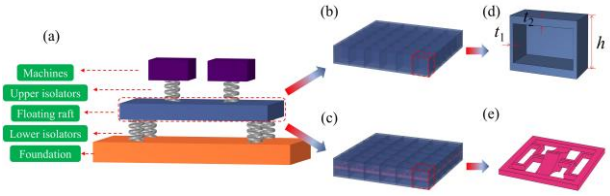

Figure 5. Schematic diagram of floating raft system with (b) honeycomb metamaterial raft and (c) sandwich metamaterial raft based on FC-ABH. (d) Cross-section of the honeycomb microunit. (e) Stereogram of FC-ABH.

Table 2. Structural parameters of the microunit of the raft. E_4, ρ_4, ν_4 are elastic modulus, density and Poisson's ratio of structural steel respectively.

Parameters	Value[unit]	Parameters	Value[unit]
h	0.026[m]	E_4	200[GPa]
t_1	1.05[mm]	ρ_4	7850[kg/m^3]
t_2	0.003[m]	ν_4	0.3

4.2 Load-bearing analysis

In this study, the equivalent elastic modulus of a sample consisting of 2×2 microunits is calculated to predict the mechanical properties of the two types of floating rafts. As we focus on the out-of-plane compression resistance of the proposed model, the elastic modulus E_z along the z direction is investigated as follows. As shown in Fig. 6(a), two rigid plates are connected with the top and bottom surface of the structure to simulate the test in practice. The bottom plate is fixed and a displacement with amplitude U_0 is applied to the top one in the negative direction of z axis. The stress-strain curve is obtained by sweeping U_0 from 0 to 0.3 mm, and the values of the stress and strain at a certain U_0 are derived as Eqns. (9) and (10), where F_r denotes the boundary reactive force at the surface that contact with the top rigid plate, and

∫.dS means that the integration is taken over the entire top surface.

$$\sigma = \frac{\int_S F_r dS}{\left[2(a+2t_1)\right]^2} \tag{9}$$

$$\varepsilon = \frac{U_0}{h} \tag{10}$$

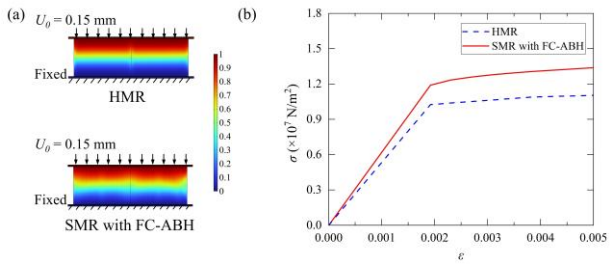

Figure 6. (a) Displacement fields of the sample of the raft in compression simulation when U_0 = 0.15 mm. (b) Stress-strain curves of the sample with and without embedding FC-ABH.

Fig. 6(b) exhibits the simulation results. It can be observed that the linear response for both samples is similar in the initial loading, while the compressive strength of the honeycomb one reaches the peak first, with the appearance of plastic buckling. The yield elastic moduli of the samples with and without FC-ABH calculated by $E_z = \sigma/\varepsilon$ are 5.33 GPa and 6.19 GPa respectively, indicating that the sandwich design improves the static stiffness of the ordinary raft. In addition, by analyzing the displacement fields of the cross-section at the linear segment, it can be observed that the presence of the interlayer changes the distribution of displacement, and partly improves the buckling resistance.

4.3 Vibration isolation of sandwich metamaterial raft

In this subsection, the simulation model of the floating raft system is simplified as shown in Fig. 7(a), where one machine is retained to provide the excitation and the raft is composed of 6×6 sandwich microunits. The side length of the simply-supported foundation is equal to that of the raft, with thickness 0.02 m. Moreover, the upper and lower isolators are substituted by the same 0.1 m×0.1 m×0.027 m rubber pads, with material properties E_5 = 0.02 GPa, ρ_5 = 1300 kg/m^3, ν_5 = 0.47 and η_5 = 0.1. The machine model is set as a rigid domain and a sinusoidal excitation with an amplitude of 20 N is applied to the top of it. To evaluate the vibration isolation performance of the system, the vibration level difference between the machine and the foundation is calculated via Eqn. (11), where A_m and A_f represent the acceleration amplitudes of the corresponding points output-1 and output-2.

$$L_D = 20\lg\frac{A_m}{A_f} \tag{11}$$

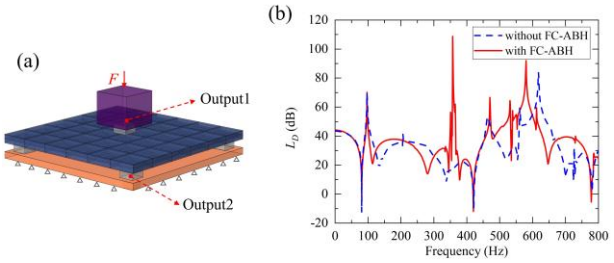

Figure 7. (a) Model of the floating raft system in simulation. (b) Vibration level differences of the floating raft system with honeycomb metamaterial raft and sandwich metamaterial raft based on FC-ABH.

Fig. 7 shows the vibration level difference results, compared with those of the system with honeycomb raft. It can be found that when using the sandwich raft, there is a more significant vibration isolation at 300-400 Hz, which is due to the locally resonant effect. In addition, beyond the locally resonant bandgap, the L_D of the system with the sandwich raft keeps higher than that with an ordinary one, especially at 480-600 Hz, which is because of the ABH absorbers. Due to the limitation of the length of the article, the vibration isolation mechanism of the sandwich raft is not analyzed in detail here. However, to reflect the vibration response of the entire system more comprehensively, the mean quadratic velocity (MQV) of the foundation and the raft surface are calculated, as in Eqn. 12, where ω is the angular frequency and ref = 1×10^{-18} m^2/s^2 [20].

$$\mathrm{MQV} = 10\lg\frac{\omega^2\iint_S w^2 dS}{\left[6(a+2t_1)\right]^2\cdot \mathrm{ref}} \tag{12}$$

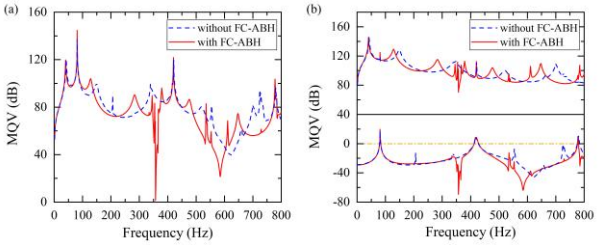

Figure 8. MQV curves of (a) the foundation plate, (b) the raft plate and the difference between them.

As displayed in Fig. 8, the sandwich raft operates at 300-600 Hz, which is consistent with the frequency band that the L_D increases significantly in Fig. 7(b). Furthermore, it can be found that the second peak of the MQV difference disappears in the system with the sandwich raft, presenting broadband vibration isolation performance.

5. CONCLUSION

This paper proposes a novel metamaterial design to achieve broadband and low-frequency vibration suppression, utilizing the coupling effects of local resonance and wave absorption of the acoustic black hole (ABH). The dispersion relation of the infinite periodic structure and the vibration bandgap of the finite periodic plate are calculated, verified by the experimental results. The ABH part acts as a vibration absorber as well as a resonator, allowing vibration to be well attenuated even beyond the bandgap.

After the monomer is analyzed, its application to the floating raft system is studied. The microunit is used as a core layer embedded into a honeycomb plate-type raft periodically. Out-of-plane compression process reveals that the sandwich raft exhibits improved static stiffness, which can meet the requirement of large load-bearing capacity in practical applications. Compared with the conventional floating raft system, the vibration level difference of the one with the proposed sandwich raft is significantly improved in vibration bandgaps, demonstrating low-frequency and broadband vibration isolation performance.

This study offers an effective design with superior static and dynamic properties. The proposed meta-structure may provide a new strategy for ship-vibration technologies.

6. ACKNOWLEDGMENTS

This work is supported by the National Natural Science Foundation of China (No. 12132010, No. 12202304), and S&T Program of Hebei (225676162GH).

7. REFERENCES

[1] M. A. Mironov: "Propagation of a flexural wave in a plate whose thickness decreases smoothly to zero in a finite interval," *Sov Phys Acoust*, vol. 34, no. 3, pp. 318-319, 1988.

[2] A. Pelat, F. Gautier, S. C. Conlon, et al.: "The acoustic black hole: A review of theory and applications," *Journal of Sound and Vibration*, vol. 476, no. 115316, 2020.

[3] T. Zhou and L. Cheng: "A resonant beam damper tailored with Acoustic Black Hole features for broadband vibration reduction," *Journal of Sound and Vibration*, vol. 430, pp. 174-184, 2018.

[4] K. X. Huang, Y. N. Zhang, X. T. Rui, et al.: "A multibody dynamics approach on a tree-shaped acoustic black hole vibration absorber," *Applied Acoustics*, vol. 210, no. 109439, 2023.

[5] H. L. Ji, N. Wang, C. Zhang, et al.: "A vibration absorber based on two-dimensional acoustic black holes," *Journal of Sound and Vibration*, vol. 500, no. 116024, 2021.

[6] H. Sheng, M. X. He and Q. Ding: "Vibration control and multifunctional design based the acoustic black hole structure: a state-of-the-art review," *International Journal of Dynamics and Control*, vol. 13, no. 25, pp. 1-20, 2025.

[7] S. T. Hao, H. Sheng, X. S. Liu, et al.: "Low-frequency and broadband vibration absorption of a metamaterial plate with acoustic black hole resonators," *Thin-Walled Structures*, vol. 202, no. 112073, 2024.

[8] J. Deng, J. F. Ma, X. Chen, et al.: "Vibration damping by periodic additive acoustic black holes," *Journal of Sound and Vibration*, vol. 574, no. 118235, 2024.

[9] J. Deng, N. S. Gao, X. Chen, et al.: "Evanescent waves in a metabeam attached with lossy acoustic black hole pillars," *Mechanical Systems and Signal Processing*, vol. 191, no. 110182, 2023.

[10] H. Sheng, M. X. He and Q. Ding: "Vibration suppression by mistuning acoustic black hole dynamic vibration absorbers," *Journal of Sound and Vibration*, vol. 542, no. 117370, 2022.

[11] L. L. Ren, Y. Li, X. C. Huang, et al.: "Dynamic Modeling and Characteristic Analysis of Floating Raft System with Attached Pipes," *Shock and Vibration*, vol. 2017, pp. 1-13, 2017.

[12] H. L. Sun, K. Zhang, P. Q. Zhang, et al.: "Application of dynamic vibration absorbers in floating raft system," *Applied Acoustics*, vol. 71, pp. 250-257, 2010.

[13] Z. Wang and C. M. Mak: "Application of a movable active vibration control system on a floating raft," *Journal of Sound and Vibration*, vol. 414, pp. 233-244, 2018.
[14] Y. L. Li and D. L. Xu: "Force transmissibility of floating raft systems with quasi-zero-stiffness isolators," *Journal of Vibration and Control*, vol. 24, no. 16, pp. 3608-3616, 2017.
[15] H. L. Wang, M. Li, Y. C. Zeng, et al.: "Experimental, theoretical and optimization studies on multimode vibration reduction of floating raft system based on NES cells," *Ocean Engineering*, vol. 311, no. 118897, 2024.
[16] Y. B. Song, J. H. Wen, D. L. Yu, et al.: "Suppression of vibration and noise radiation in a flexible floating raft system using periodic structures," *Journal of Vibration and Control*, vol. 21, no. 2, pp. 217-228, 2013.
[17] X. Y. An, X. F. Yuan, G. Q. Sun, et al.: "Sandwich plate-type metastructures with periodic graded resonators for low-frequency and broadband vibration attenuation," *Ocean Engineering*, vol. 298, no. 117229, 2024.
[18] J. Deng, L. Zheng and N. S. Gao: "Broad band gaps for flexural wave manipulation in plates with embedded periodic strip acoustic black holes," *International Journal of Solids and Structures*, vol. 224, no. 111043, 2021.
[19] J. Deng, O. Guasch and L. Zheng: "Ring-shaped acoustic black holes for broadband vibration isolation in plates," *Journal of Sound and Vibration*, vol. 458, pp. 109-122, 2019.
[20] S. T. Wen, M. X. Chen, Z. W. Zhou, et al.: "Analytical and experimental studies for the vibration transmission of the double-plated structure containing the inner fluid and elastic connections," *Thin-Walled Structures*, vol. 188, no. 110806, 2023.